Human Molecular Genetics, 2008, Vol. 17, No. 1 **71–86**
doi:10.1093/hmg/ddm285
Advance Access published on September 28, 2007

A novel Usher protein network at the periciliary reloading point between molecular transport machineries in vertebrate photoreceptor cells

Tina Maerker[1], Erwin van Wijk[2,3], Nora Overlack[1], Ferry F.J. Kersten[2,3,4,5], JoAnn McGee[6], Tobias Goldmann[1], Elisabeth Sehn[1], Ronald Roepman[3,5], Edward J. Walsh[6], Hannie Kremer[2] and Uwe Wolfrum[1,*]

[1]Department of Cell and Matrix Biology, Institute of Zoology, Johannes Gutenberg University of Mainz, 55099 Mainz, Germany, [2]Department of Otorhinolaryngology, [3]Department of Human Genetics, [4]Department of Ophthalmology and [5]Nijmegen Centre for Molecular Life Sciences, Radboud University Nijmegen Medical Centre, 6500 HB Nijmegen, The Netherlands and [6]Developmental Auditory Physiology Laboratory, Boys Town National Research Hospital, Omaha, NE 68131, USA

Received August 21, 2007; Revised and Accepted September 27, 2007

The human Usher syndrome (USH) is the most frequent cause of combined deaf–blindness. USH is genetically heterogeneous with at least 12 chromosomal loci assigned to three clinical types, USH1–3. Although these USH types exhibit similar phenotypes in human, the corresponding gene products belong to very different protein classes and families. The scaffold protein harmonin (USH1C) was shown to integrate all identified USH1 and USH2 molecules into protein networks. Here, we analyzed a protein network organized in the absence of harmonin by the scaffold proteins SANS (USH1G) and whirlin (USH2D). Immunoelectron microscopic analyses disclosed the colocalization of all network components in the apical inner segment collar and the ciliary apparatus of mammalian photoreceptor cells. In this complex, whirlin and SANS directly interact. Furthermore, SANS provides a linkage to the microtubule transport machinery, whereas whirlin may anchor USH2A isoform b and VLGR1b (very large G-protein coupled receptor 1b) via binding to their cytodomains at specific membrane domains. The long ectodomains of both transmembrane proteins extend into the gap between the adjacent membranes of the connecting cilium and the apical inner segment. Analyses of Vlgr1/del7TM mice revealed the ectodomain of VLGR1b as a component of fibrous links present in this gap. Comparative analyses of mouse and *Xenopus* photoreceptors demonstrated that this USH protein network is also part of the periciliary ridge complex in *Xenopus*. Since this structural specialization in amphibian photoreceptor cells defines a specialized membrane domain for docking and fusion of transport vesicles, we suggest a prominent role of the USH proteins in cargo shipment.

INTRODUCTION

Vertebrate rod and cone photoreceptor cells are highly polarized neurons, which consist of morphological and functional distinct cellular compartments. A light sensitive outer segment is linked via a non-motile connecting cilium with an inner segment, which contains the organelles typical for the metabolism of eukaryotic cells. The outer segment is characterized by specialized flattened disk-like membranes, where all components of the visual transduction cascade are arranged. These phototransductive membranes in the outer segment are continually renewed throughout lifetime. Newly synthesized membranes are added at the base of the outer segment, whereas disks at the outer segment apex are

*To whom correspondence should be addressed at: Department of Cell and Matrix Biology, Institute of Zoology, Johannes Gutenberg University of Mainz, Muellerweg 6, D-55099 Mainz, Germany. Tel: +49 61313925148; Fax: +49 61313923815; Email: wolfrum@uni-mainz.de

© *The Author 2007. Published by Oxford University Press. All rights reserved.*
For Permissions, please email: journals.permissions@oxfordjournals.org

phagocytosed by cells of the retinal pigment epithelium (1). All molecular components of the outer segment machinery are synthesized in organelles located in the basal part of the inner segment and are vectorially transported in the inner segment and through the connecting cilium to the outer segment (2–4). On its route, the cargo has to be reloaded from inner segment transport carriers to ciliary transport systems in a specialized compartment of the apical inner segment (5). In our present study, we identified a protein network which participates in the cargo delivery from the inner segment to the outer segment of vertebrate photoreceptor cells. Interestingly, the proteins of this network are encoded by genes related to the human Usher syndrome (USH).

The USH is an autosomal recessive disorder characterized by combined hearing loss and retinal degeneration. USH is genetically heterogeneous with at least 12 chromosomal loci involved. Depending on their clinical features (onset, severity and progression) three USH types can be distinguished (6–8). Patients suffering from USH1, the most severe form, exhibit profound congenital hearing loss and constant vestibular dysfunction, combined with pre-pubertal onset of retinitis pigmentosa. In USH2, the most frequent type, congenital hearing loss is milder; the onset of retinitis pigmentosa is during or after puberty and vestibular function remains normal. USH3 is only relatively frequent in specific populations and characterized by progressive hearing loss with variability in vestibular dysfunction and in the onset of retinitis pigmentosa.

The gene products of identified USH genes belong to various protein classes and families as recently reviewed in Reiners *et al*. (9) and Kremer *et al*. (10): USH1B encodes the molecular motor myosin VIIa; harmonin (USH1C), SANS (scaffold protein containing ankyrin repeats and SAM domain, USH1G) and whirlin, more recently identified as USH2D (11) belong to the group of scaffold proteins (Fig. 1A); cadherin 23 (USH1D) and protocadherin 15 (USH1F) represent cell–cell adhesion proteins, whereas USH2A and USH2C encode the large transmembrane protein USH2A isoform b and seven transmembrane receptor VLGR1b (very large G-protein coupled receptor 1b), respectively (Fig. 1A). The four-transmembrane-domain protein clarin-1 (USH3A) is so far the only member of USH3.

Previous molecular analyses revealed that the USH1C scaffold protein harmonin integrates all USH1 and USH2 proteins into USH protein networks [see recent reviews (9,10)]. In hair cells of the inner ear, harmonin mediated USH protein networks are thought to be essential for stereocilia development and may participate in synaptic function as well as in mechano-electric signal transduction (6,9,10). In the retina, the function of these protein networks is mainly assumed to maintain synaptic integrity and function (9).

However, the USH proteins SANS and whirlin were already suggested as scaffold proteins organizing additional protein networks in the inner ear and the retina (10,12–14). SANS forms homodimers and directly interacts with harmonin and myosin VIIa (12). In the present study, direct binding of SANS and whirlin was confirmed as originally suggested (10,14). In addition, we found evidence for the association of SANS with the microtubule cytoskeleton. In previous studies, we demonstrated direct interaction of whirlin with the cytoplasmic domains of USH2A isoform b and VLGR1b (10,14). The latter transmembrane proteins were proposed as molecular components of fibrous ankle links between adjacent stereocilia of mechanosensitive hair cells (13,15). A more recent study demonstrated whirlin as the major scaffold protein of a USH protein network in the ankle link complex of inner ear hair cells (16). Immunological analyses indicated that the ankle links between neighboring stereocilia of hair cells share antigens with fibrous links localized in the gap between the adjacent membranes of the inner segment apex and the connecting cilium of vertebrate photoreceptor cells (15,17,18). Here, we describe a novel USH protein network in the periciliary region of vertebrate photoreceptor cells, which has a molecular composition comparable to the ankle link complex. We show that the ectodomain of VLGR1b is an essential component of the fibrous links connecting the adjacent membranes in the ciliary region of photoreceptor cells. Furthermore, our comparative analyses of mouse and *Xenopus* photoreceptor cells provide strong indications for an important role of this novel periciliary USH protein complex in the delivery of cargo to the outer segment of vertebrate photoreceptor cells in general.

RESULTS

The USH1G protein SANS directly interacts with the USH2D protein whirlin

Yeast two-hybrid screens were performed to identify proteins interacting with the USH1G protein SANS. For this, the C-terminus of human SANS (amino acids 400–465) containing a sterile alpha motif (SAM) domain and a class I PDZ-binding motif (PBM) (Fig. 1A) was used as a bait to screen a bovine retina cDNA library. Of the 40 positive clones encoding potential interaction partners 33 encoded the N-terminal region of whirlin. Reciprocal yeast two-hybrid assays confirmed specific interaction between whirlin and the C-terminus of SANS and pinpointed the binding site of the whirlin molecule to its PDZ domains 1 and 2 (Fig. 1B).

In order to validate the SANS–whirlin interaction, different recombinant expressed domains of both proteins were used to carry out glutathione *S*-transferase (GST) pull-down assays. Incubation of GST-tagged whirlin PDZ domains, namely PDZ1, PDZ2, PDZ1 and 2, PDZ3 or GST alone with FLAG-tagged full-length SANS identified whirlin's PDZ1 and 2 as the binding sites for SANS (Fig. 1C). Interaction of FLAG-tagged SANS and whirlin's PDZ3 or GST alone could not be detected. In GST pull-down assays with the FLAG-tagged C-terminal SAM domain of SANS lacking the PBM motif (FLAG–SANS SAMΔPBM) the interaction was abolished (Fig. 1C). Since the N-terminal 400 amino acids of SANS were not present in the bait construct used in our initial yeast-two hybrid screen these findings strongly support that SANS directly interacts via its C-terminal PBM motif with PDZ1 and PDZ2 of whirlin.

To confirm this interaction *in vivo*, COS-1 cells were cotransfected with plasmids encoding full-length SANS and the long isoform of whirlin fused to eCFP or mRFP, respectively (Fig. 1D). In mRFP–whirlin transfected COS-1 cells, the mRFP-fluorescence was present in the entire cytoplasm

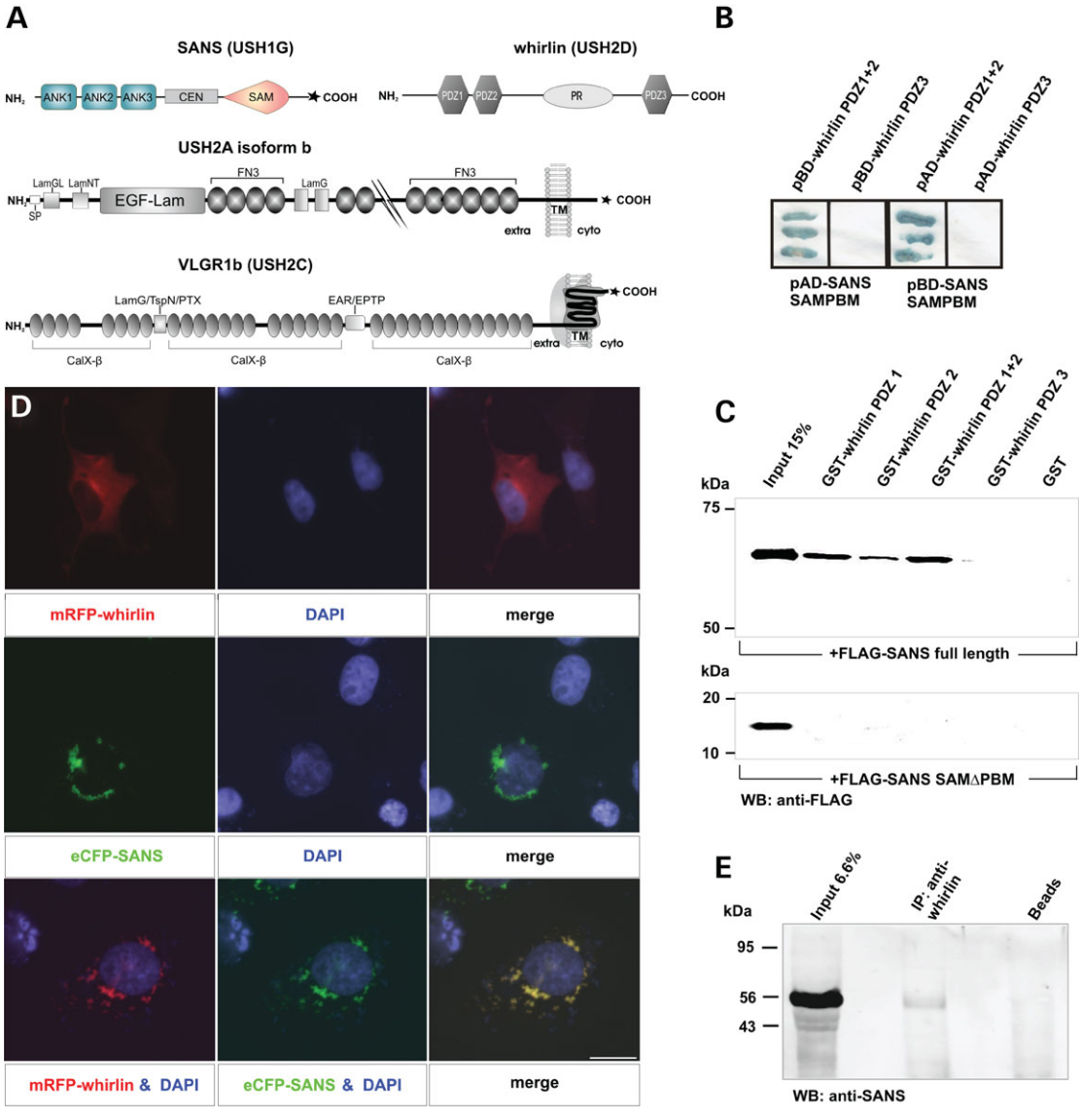

Figure 1. Validation of the SANS–whirlin interaction. (**A**) Schematic representation of SANS, whirlin, USH2A isoform b and VLGR1b. SANS is composed of three ankyrin repeats (ANK) at the N-terminus, a central domain (CEN) followed by a sterile alpha motif (SAM) and a PDZ-binding motif (PBM) at the C-terminus indicated by an asterisk. Whirlin contains three PDZ domains and a proline-rich region (PR). The extracellular domain of the USH2A isoform b (USH2A) contains a laminin G-like domain (LamGL), an N-terminal laminin domain (LamNT), 10 laminin-type EGF-like modules (EGF-Lam), 32 fibronectin type III (FN3) repeats (4+28) spaced by two laminin G domains (LamG) followed by a transmembrane region (TM) and the intracellular C-terminal domain containing a PBM. VLGR1b (very large G-protein coupled receptor 1b, USH2C) consists of extracellular N-terminal extensions with a LamG/TspN/PTX-homologous domain, seven EAR/EPTP repeats, 35 Ca^{2+}-binding calcium exchanger β (CalX-β) modules, one 7-transmembrane domain (TM) as well as a short intracellular domain containing a PBM. (**B**) Reciprocal yeast two-hybrid interaction assays were performed with the SANS C-terminus containing the SAM and PBM domains and whirlin's PDZ1+2 or PDZ3 fused to the activation domain (pAD) or the DNA-binding domain (pBD) of the GAL4 reporter gene, respectively. SANS interacts with whirlin's PDZ1+2, but not with the PDZ3 domain. (**C**) GST pull-down assays were performed: upper panel, FLAG-tagged SANS is incubated with immobilized GST-whirlin PDZ domains, or GST alone. Anti-FLAG western blot reveals recovery of SANS with whirlin PDZ1, PDZ2 and PDZ1+2, but not with whirlin's PDZ3 or GST alone. Lower panel, FLAG-tagged SANS C-terminus lacking the PBM (SAMΔPBM) is assayed with each of the immobilized GST-tagged PDZ-domains of whirlin or GST protein alone and analyzed by anti-FLAG western blot analysis. Binding of SANS to whirlin is abolished. (**D**) Colocalization of recombinant mRFP–whirlin and eCFP–SANS in COS-1 cells. upper panel: overexpressed mRFP–whirlin (red) is localized to the cytoplasm but not to the DAPI stained nucleus in single transfected cells. middle panel: overexpressed eCFP–SANS (green) is localized to punctuated structures in the periphery of the nucleus. lower panel: in mRFP–whirlin and eCFP–SANS double transfected COS-1 cells, overexpressed eCFP–SANS (green) recruits mRFP–whirlin (red) to the perinuclear punctuated structures. Scale bar: 10 μm. (**E**) Immunoprecipitation (IP) with anti-whirlin antibodies of protein extract of mouse retinas. Anti-SANS western blot analysis (WB) demonstrates that SANS is coimmunoprecipitated with whirlin. In protein AG-Beads (Beads) incubated retinal extracts SANS is not recovered.

with a concentration in the perinuclear area (Fig. 1D, upper panel). ECFP–SANS single transfected cells expressed the fusion protein in granulous aggregates in the periphery of the nucleus (Fig. 1D, middle panel). In cotransfected COS-1 cells, mRFP–whirlin and eCFP–SANS were colocalized in these granules in the periphery of the nucleus

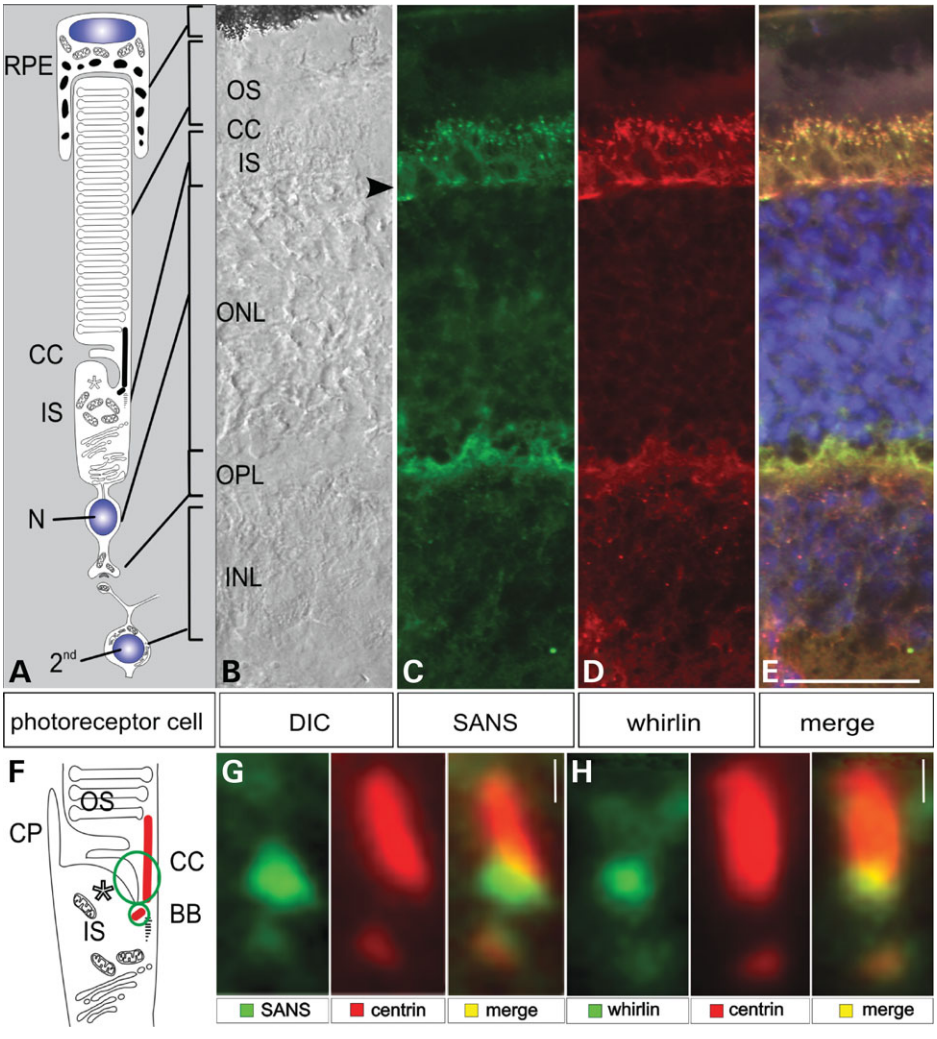

Figure 2. SANS and whirlin colocalize in mouse photoreceptor cells. (**A**) Schematic representation of a rod photoreceptor cell. Vertebrate photoreceptors are composed of a light-sensitive outer segment (OS) linked via a connecting cilium (CC) to an inner segment (IS), containing all organelles for biosynthesis. N, nucleus localized in the outer nuclear layer (ONL); Photoreceptor synaptic terminals located in the outer plexiform layer (OPL) of the retina. Arrowhead points to outer limiting membrane (OLM). 2nd, second order neurons, bipolar or horizontal cells, respectively. RPE, retinal pigment cells. (**B**–**E**) Indirect immunofluorescence double labeling of SANS and whirlin counterstained with DAPI in a longitudinal cryosection through a mouse retina. (B) Differential interference contrast (DIC) image of C–E. (C and D) Indirect immunofluorescence of SANS (green) (C) and whirlin (red) (D). (E) Merge image of SANS and whirlin labeling superposed with the nuclear DNA staining by DAPI. The yellow color indicates SANS and whirlin colocalization in the CC, the IS, the OLM and the OPL in photoreceptor cells. (**F**) Schematic representation of the ciliary apparatus composed of the connecting cilium (CC) and the basal body complex (BB) in a rod photoreceptor cell. CP, calycal processes. (**G** and **H**) High magnification fluorescence microscopy analyses of double immunofluorescence with anti-SANS or anti-whirlin, respectively, and anti-pan-centrin antibodies (marker for the ciliary apparatus: CC and BB) in longitudinal cryosections through the ciliary part of mouse photoreceptor cells. (G) Double labeling of SANS (green) and centrins (red). (H) Double labeling of whirlin (green) and centrins (red). Merged images indicate partial colocalization of SANS and whirlin with centrins in the CC and the BB. The periciliary collar-like inner segment (IS) extension is indicated by an asterisk. Scale bars: (E) 20 μm, (G and H) 0.2 μm.

(Fig. 1D, lower panel) indicating a recruitment of mRFP–whirlin towards the nucleus through its interaction with eCFP–SANS. To evaluate whether the interaction between SANS and whirlin also occurs in the retina, coimmunoprecipitations were performed. For this purpose, extracts of mouse retinas were incubated with anti-whirlin antibodies immobilized on agarose beads. Western blot analysis of the immunoprecipitates with anti-SANS antibodies revealed coimmunoprecipitation of SANS with whirlin (Fig. 1E). In conclusion, the results of the present protein–protein interaction analyses indicate specific binding of SANS via its C-terminal class I PBM to the PDZ domains 1 and 2 of whirlin.

Subcellular colocalization of the USH scaffold proteins SANS and whirlin in the ciliary region of mouse photoreceptor cells

In situ protein–protein interaction of SANS and whirlin should imply colocalization of both binding partners in tissue. To validate this, we carried out indirect immunofluorescence double labeling experiments with anti-SANS and anti-whirlin antibodies in murine retinal cryosections. Double immunofluorescence labeling revealed colocalization of SANS and whirlin at the synapses in the outer plexiform layer, in the outer limiting membrane, the inner segment and the ciliary

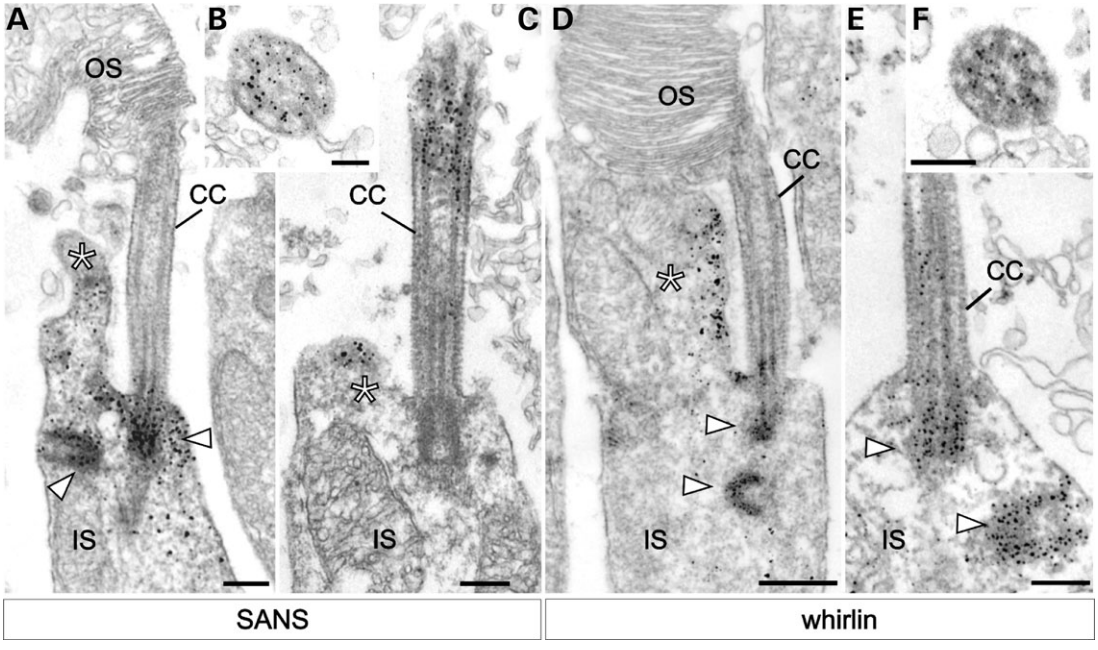

Figure 3. Immunoelectron microscopic localization of SANS and whirlin in mouse photoreceptor cells. (**A**–**C**) Electron micrographs of anti-SANS labeling in longitudinal (A and C) and cross-sections (B) through parts of mouse photoreceptor cells. SANS localization is found in the apical inner segment (IS) in the periciliary collar-like extension (asterisk) and at the basal body complex (arrow heads). In some longitudinal sections (C) and in cross-sections (B), SANS is also detected in the connecting cilium (CC). (**D**–**F**) Electron micrographs of anti-whirlin labeling in longitudinal (D and E) and cross-sections (F) through parts of mouse photoreceptor cells. Whirlin is localized in the apical IS in the periciliary collar-like IS extension (asterisk) and at the basal body complex (arrow heads). In some longitudinal sections (E) and in cross-sections (F), whirlin is also detected in the CC. Scale bars: (A) 0.25 μm, (B) 0.1 μm, (C) 0.25 μm, (D) 0.5 μm (E) 0.25 μm and (F) 0.2 μm.

region of photoreceptor cells (Fig. 2C–E). For further confirmation of the localization of SANS and whirlin in the ciliary apparatus of photoreceptor cells, immunofluorescence double labeling with antibodies against SANS or whirlin, respectively, and anti-pan-centrin antibodies, a well characterized molecular marker for the photoreceptor ciliary apparatus (19,20), was performed. High resolution analyses of double immunofluorescences revealed colocalization of SANS and whirlin in the connecting cilium and the basal body complex of photoreceptor cells (Fig. 2F–H).

To elucidate the subcellular distribution of SANS and whirlin more precisely in mouse photoreceptors, we performed immunoelectron microscopy. Pre-embedding immunolabeling with anti-SANS and anti-whirlin antibodies confirmed the localization of both proteins in the connecting cilium, the basal body complex and in the apical inner segment of mouse photoreceptor cells (Fig. 3). It is important to note, that the pre-embedding immunoelectron microscopy analyses of SANS and whirlin in the connecting cilium depended on the depth of the antibody penetration into the connecting cilium. Therefore, concentrations of antibody staining were found in the proximal and apical portion of the cilium to which the antibodies were able to freely diffuse (Figs 3 and 4). However, since the ciliary membrane turned out to be often resistant to the cracking procedure and detergent treatments applied (21), antibodies were unable to penetrate the ciliary membrane and therefore the middle portion of the cilium was seldom stained. Nevertheless, in other photoreceptor cells the ciliary region was more perforated. In those cases, antibodies were able to reach the ciliary cytoplasm and the antigen epitopes present in the cilium were detected (Fig. 3 B, C, E and F). Exploiting the high resolution of the electron microscope, we demonstrated labeling of SANS and whirlin pronounced in the cytoplasm of the apical inner segment extension (Fig. 3A, C and D). This extension forms a collar alongside the connecting cilium and is different from calycal processes, which project as slender elongations of the inner segment apex along the outer segment (22).

Since harmonin was previously shown as the major scaffold protein organizing USH protein networks (9,10), we analyzed the subcellular localization of harmonin by a spectrum of equivalent methods. Immunofluorescence analyses and immunelectron microscopy after pre-embedding labeling confirmed our previous results (23). Harmonin was localized at the synaptic region, in the inner segment and the outer segment, but was absent from in the apical collar of the inner segment and in the connecting cilium of mouse photoreceptor cells (Supplementary material Fig. S1).

Subcellular colocalization of SANS and whirlin with the cytoplasmic domains of USH2A isoform b and VLGR1b in the connecting cilium and apical inner segment collar of mouse photoreceptor cells

The USH2 proteins USH2A isoform b and VLGR1b (USH2C) are transmembrane proteins composed of a very short intracellular cytoplasmic domain and a very long extracellular ectodomain (Fig. 1A). The expression of USH2A isoform b and VLGR1b in mouse retina and previous immunofluorescence studies indicated their localization in the outer plexiform

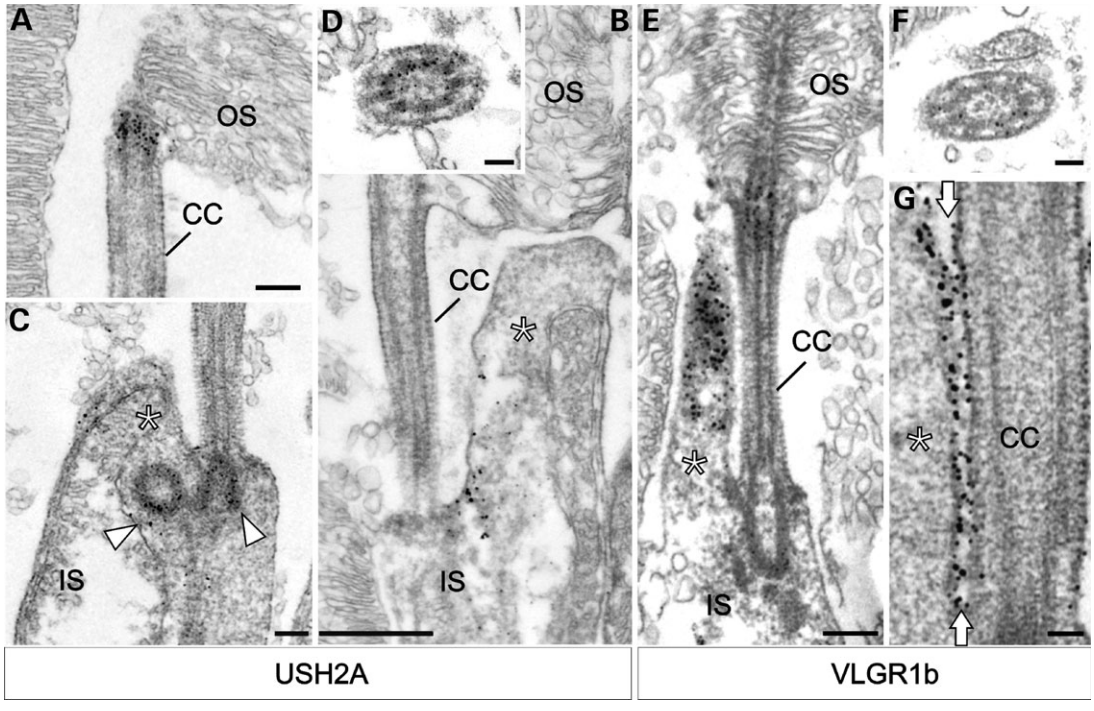

Figure 4. Immunoelectron microscopic localization of USH2A isoform b and VLGR1b in mouse photoreceptor cells. (**A**–**D**) Electron micrographs of anti-USH2A isoform b immunolabeling in longitudinal (A–C) and cross-sections (D) through parts of mouse photoreceptor cells. (A–D) USH2A isoform b localization is found in the apical inner segment (IS) in the periciliary collar-like extension (asterisk) and at the basal body complex (arrow heads in C). In some longitudinal sections (A) and in cross-sections (D) USH2A isoform b is also detected in the connecting cilium (CC). (**E**–**G**) Electron micrographs of anti-VLGR1b labeling in longitudinal (E and G) and cross- sections (F) through parts of mouse photoreceptor cells. In longitudinal sections VLGR1b labeling by antibodies directed against the intracellular domain is found in the periciliary collar-like IS extension (asterisk) and in the CC (E). Staining in the CC is also observed in cross-sections (F). (G) Anti-VLGR1b antibodies directed against the extracellular domain reveal VLGR1b localization in the gap (arrows) between membranes of the periciliary collar-like IS extension (asterisk) and the CC. Scale bars: (A) 0.25 μm, (B) 0.5 μm, (C) 0.2 μm, (D) 0.25 μm and (E and G) 0.1 μm.

layer, the inner segment and more interestingly also in the region of the connecting cilium (9,14). Furthermore, direct association of USH2A isoform b and VLGR1b with whirlin was demonstrated (13,14). Therefore, we investigated the subcellular localization of these USH2 transmembrane proteins by high resolution immunofluorescence and immunoelectron microscopy. High-magnification immunofluorescence images of double labeling of USH2A isoform b or VLGR1b, respectively and the ciliary molecular marker centrin revealed partial colocalization (Supplementary material Fig. S2). Immunofluorescence labeling of USH2A isoform b was found in the connecting cilium and the basal body complex, while VLGR1b staining was present in the connecting cilium. These results confirmed USH2A isoform b and VLGR1b as components of the ciliary apparatus (9,24).

Pre-embedding immunoelectron microscopy analyses demonstrated localization of both transmembrane proteins, SANS and whirlin in the same compartments of the photoreceptor cell, indicating the colocalization of all four proteins. Anti-USH2A antibodies directed against the intracellular domain of USH2A isoform b detected USH2A at the basal body complex, the connecting cilium and the adjacent collar of the apical inner segment of photoreceptor cells (Fig. 4A–D). Unfortunately, antibodies raised against the extracellular domain of USH2A isoform b which previously stained the ciliary region of photoreceptor cells by indirect immunofluorescence (9,14,24) did not work in our pre-embedding labeling protocol for immunoelectron microscopy analyses (data not shown). The antibodies directed against intracellular domains of VLGR1b labeled VLGR1b at the apical membrane of the inner segment and the connecting cilium of mouse photoreceptor cells (Fig. 4E and F). VLGR1b and USH2A isoform b labeling of cross-sections through connecting cilia confirmed their ciliary localization (Fig. 4D and F). Nevertheless, the staining of VLGR1b and USH2A isoform b in the connecting cilium was incomplete (see Fig. 4C, B and E) due to the methodological limitations discussed above for immunoelectron microscopy analyses for SANS and whirlin.

Ectodomains of VLGR1b are components of fibrous links bridging the ciliary and apical inner segment membrane of photoreceptor cells

The subcellular distribution of the long extracellular domain of VLGR1b was analyzed with specific antibodies directed against ectodomains of VLGR1b. Immunoelectron microscopy analyses using these antibodies revealed exclusive decoration of fibrous links localized within the gap between the membranes of the connecting cilium and the periciliary inner segment collar (Fig. 4G).

It has been demonstrated that fibrous links in photoreceptor cells as well as the homologous ankle links in inner ear hair cells are sensitive to the calcium chelator BAPTA (17,18).

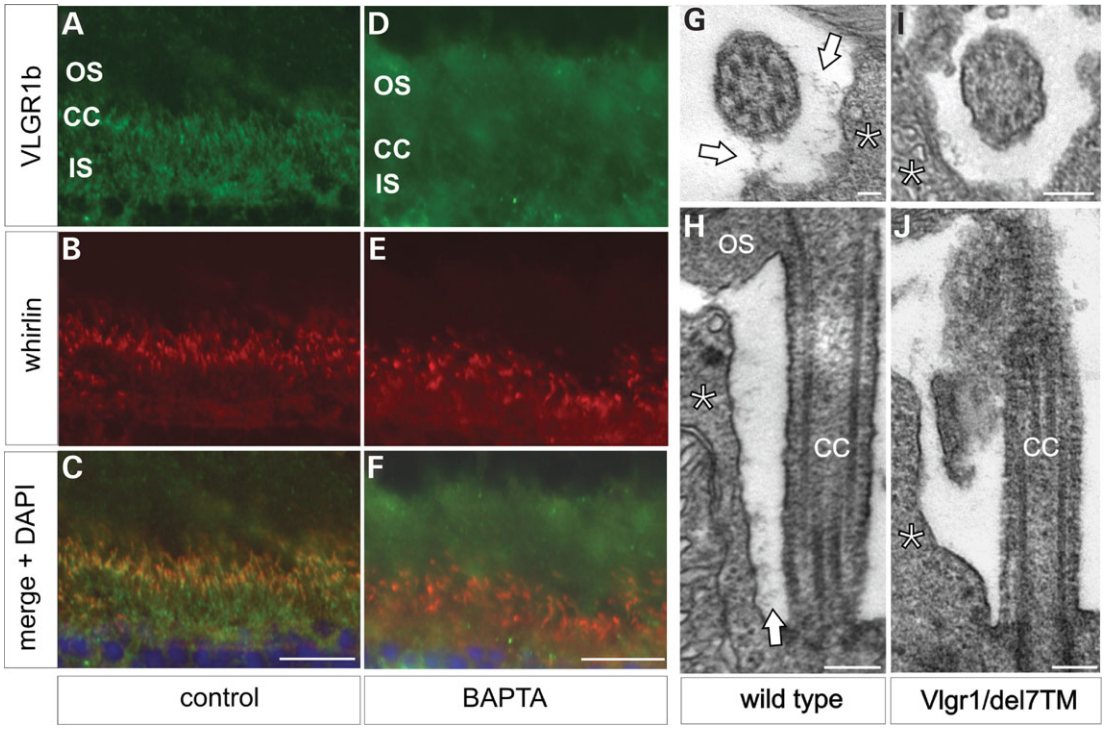

Figure 5. BAPTA sensitivity of VLGR1b ectodomains and fibrous link distribution in wild-type and Vlgr1/del7TM mouse photoreceptor cells. (**A**–**F**) BAPTA sensitivity of VLGR1b ectodomains in retinal cryosections of mouse retinas. (A–C) Double immunofluorescence labeling with antibodies directed against extracellular domains of VLGR1b and anti-whirlin antibodies of retinal cryosections, control treated with PBS. (A) Indirect immunofluorescence of anti-VLGR1b and (B) anti-whirlin antibodies. (C) Merged image of anti-VLGR1b and anti-whirlin staining superposed with nuclear DNA staining by DAPI. Anti-VLGR1b and anti-whirlin staining are localized in the ciliary region. (D–F) Double immunofluorescence labeling with antibodies directed against extracellular domains of VLGR1b and anti-whirlin antibodies of retinal cryosections after treatment with 5 mM BAPTA in PBS. (D) Indirect immunofluorescence of anti-VLGR1b and (E) anti-whirlin antibodies. (F) Merged image of anti-VLGR1b and anti-whirlin staining superposed with the nuclear staining by DAPI. After BAPTA treatment, the staining of the extracellular domain of VLGR1b is completely vanished, while anti-whirlin staining persists in the ciliary region. (**G**–**J**) Electron microscopical analyses of fibrous links in wild-type and Vlgr1/del7TM mouse photoreceptor cells. (G and H) Electron micrographs of ultrathin cross-sections (G) and longitudinal sections (H) through the ciliary region of wild-type mouse photoreceptor cells. Arrows point to the fibrous links between the adjacent membranes of the apical inner segment collar (asterisk) and the connecting cilium (CC). (I and J) Electron micrographs of ultrathin cross-sections (I) and longitudinal sections (J) through the ciliary region of homozygous Vlgr1/del7TM mouse photoreceptor cells. Fibrous links are not detectable, neither in cross-sections nor in longitudinal sections through the ciliary region of photoreceptor cells of homozygous Vlgr1/del7TM mice. Scale bars: (C and F) 20 μm; (G) 0.1 μm and (H–J) 0.2 μm.

This prompted us to test, whether the ectodomains of VLGR1b are BAPTA sensitive. For this purpose we treated retina cryosections with 5 mM BAPTA in phosphate-buffered saline (PBS) previous to immunohistochemical analyses with anti-ecto-VLGR1b or control antibodies. The VLGR1b ectodomains were BAPTA sensitive and could no longer be detected by anti-ecto-VLGR1b antibodies after treatment with BAPTA for 30 min (Fig. 5D and F). In contrast, the staining with control antibodies to whirlin and to the cytoplasmic domain of VLGR1b remained unaffected (see whirlin staining in Fig. 5E and F). These findings strengthened the hypothesis that the ectodomains of VLGR1b are components of fibrous membrane linkages in photoreceptor cells.

Fibrous links between the ciliary and apical inner segment membrane are absent in Vlgr1/del7TM mice

These results encouraged us to analyze the organization of the periciliary apparatus in VLGR1b deficient (Vlgr1/del7TM) mice. Transmission electron microscopy was used to examine the distribution of fibrous membrane linkers in retinal photoreceptor cells of wild-type and homozygous Vlgr1/del7TM mice (25). In photoreceptor cells of wild-type mice, fibrous membrane linkers were readily visible spanning the gap between the adjacent membranes (Fig. 5G and H). In contrast, these fibrous links were not detected in any of the photoreceptor cells examined from homozygous Vlgr1/del7TM mice, neither in rod (Fig. 5I and J), nor in cone photoreceptor cells (data not shown). In longitudinal ultrathin sections through the photoreceptor cells of homozygous Vlgr1/del7TM mice, the membranes of the connecting cilium and the inner segment collar were no longer closely opposed (Fig. 5J). These findings support the results described above, further strengthening the hypothesis that VLGR1b is a component of fibrous membrane linkers within the newly identified periciliary network in photoreceptor cells.

SANS, whirlin, USH2A isoform b and VLGR1b colocalize in the periciliary ridge complex of *Xenopus* photoreceptor cells

Our results from protein–protein interaction assays (14) and our immunoelectron microscopical data indicate the localization of an USH protein complex, composed of SANS,

whirlin, USH2A isoform b and VLGR1b in the connecting cilium and in the adjacent collar-like extension of the apical inner segment in mouse photoreceptor cells. To date, little was known about structural and molecular specializations in the apical inner segment subarea of mammalian photoreceptor cells. However, in amphibians, Papermaster and co-workers previously described the so-called periciliary ridge complex as a highly specialized subcellular compartment in the apex of the photoreceptor cell inner segment (26–28). A schematic representation of the periciliary ridge complex is shown in the Supplemental material Figure S3. The topologic parallels of the periciliary ridge complex to the apical inner segment membrane in mouse photoreceptor cells prompted us to analyze the subcellular distribution of SANS, whirlin, USH2A isoform b and VLGR1b in photoreceptor cells of *Xenopus laevis* by immunoelectron microscopy. Our studies revealed the localization of all four analyzed USH proteins in the ciliary apparatus and the periciliary ridge complex of *Xenopus* rod and cone photoreceptor cells (Figs 6 and 7; Supplemental material Fig. S3). In the ciliary apparatus immunolabelings were obtained in the cytoplasm of the connecting cilium and its apical projection into the outer segment (Figs 6A–C and 7A–D). Furthermore, SANS, whirlin and USH2A isoform b were found at the basal body at the base of the connecting cilium (Figs 6A–C and 7A). In the periciliary ridge complex, labeling was predominantly present in the ridges (Figs 6D and 7B and D). From these ridges fibrous links bridge to the ciliary membrane (Figs 6D and 7B and D). In contrast, the intercalating periciliary grooves which are thought to constitute the docking sites for transport vesicles were not stained by any of the antibodies (Fig. 6D).

The observed colocalization of SANS, whirlin, USH2A isoform b and VLGR1b in mouse and *Xenopus* photoreceptors confirms the presence of a periciliary USH protein network at adjacent membranes of the connecting cilium and a specialized micro compartment of the apical inner segment (Fig. 8, Supplemental material Fig. S3). Furthermore, we found first evidence for the presence of this USH protein network in calycal processes of *Xenopus* rod and cone photoreceptor cells (data not shown).

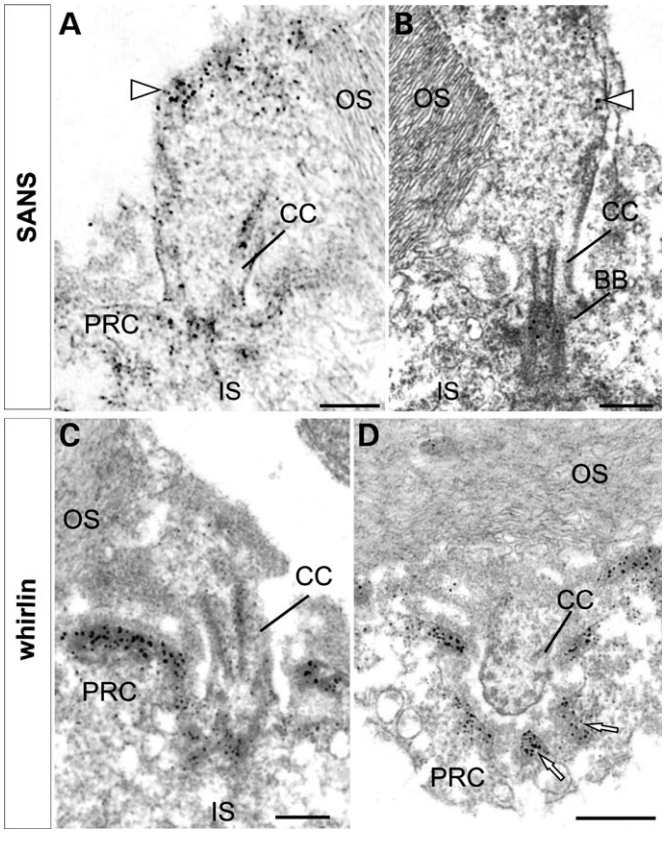

Figure 6. Subcellular localization of SANS and whirlin in *Xenopus* retina. (**A** and **B**) Electron micrographs of anti-SANS labeling in longitudinal sections of *Xenopus* photoreceptor cells. SANS localization is found in the apical inner segment (IS), in the periciliary ridge complex (PRC) at the base of the connecting cilium (CC), in the CC, in the basal body complex (BB) and in the axonemal extension of the CC (arrow head). (**C** and **D**) Electron micrographs of anti-whirlin labeling in a longitudinal section (C) and a slightly oblique cross-section through the CC and the PRC (D) of *Xenopus* photoreceptor cells. Whirlin labeling is predominantly found in the ridges of the PRC and to lesser extent in the IS and the CC. Arrows indicate the ridges of the PRC. OS, outer segment. Scale bars: (A) 0.25 μm, (B) 0.2 μm, (C) 0.25 μm and (D) 0.5 μm.

SANS is associated with microtubules in NIH3T3 and retinal photoreceptor cells

Findings from previous studies in which SANS was localized in microtubule-rich regions of inner ear hair cells and in cultured cells (12,29) prompted us to analyze a potential connection of SANS to microtubules. To illuminate the possible association of SANS with microtubules we treated cultured cells and organotypic retina cultures with microtubule destabilizing drugs. Immunofluorescence analyses of NIH3T3 cells revealed localization of endogenously expressed SANS in a perinuclear region at the centrosome of the cell (Fig. 9A; see also 29). Treatment with either colchicine or thiabendazole resulted in the degradation of the microtubule cytoskeleton (Fig. 9B and C) and caused apparent changes of the cellular distribution of SANS (Fig. 9B and C). SANS staining was no longer present at centrosomes, but was dispersed throughout the entire cytoplasm (Fig. 9B) or even found in nuclei of NIH3T3 cells (Fig. 9C).

Since our interest focused on a possible SANS association with microtubules in the retinal photoreceptor cells, we analyzed the distribution of SANS in dimethyl sulfoxide (DMSO) treated and cytoskeletal drug-treated organotypic cultures of mature mouse retinas which we recently introduced (30). Indirect immunofluorescence of cryosections through cultured mouse retinas stained by anti-SANS and anti-α-tubulin antibodies revealed a partially overlapping staining pattern of microtubules and SANS in DMSO-treated control retinas (Fig. 9D). As expected, microtubules were depolymerized after application of thiabendazole to cultured retinas (Fig. 9E, middle panel). In addition, treatments with the microtubule destabilization drug resulted in an altered distribution of SANS or even in fading of the SANS staining in photoreceptor cells (Fig. 9E). The localization of SANS in microtubule-rich regions of different cell types and its microtubule-dependent cellular distribution indicated a direct or indirect association of SANS with the microtubule cytoskeleton.

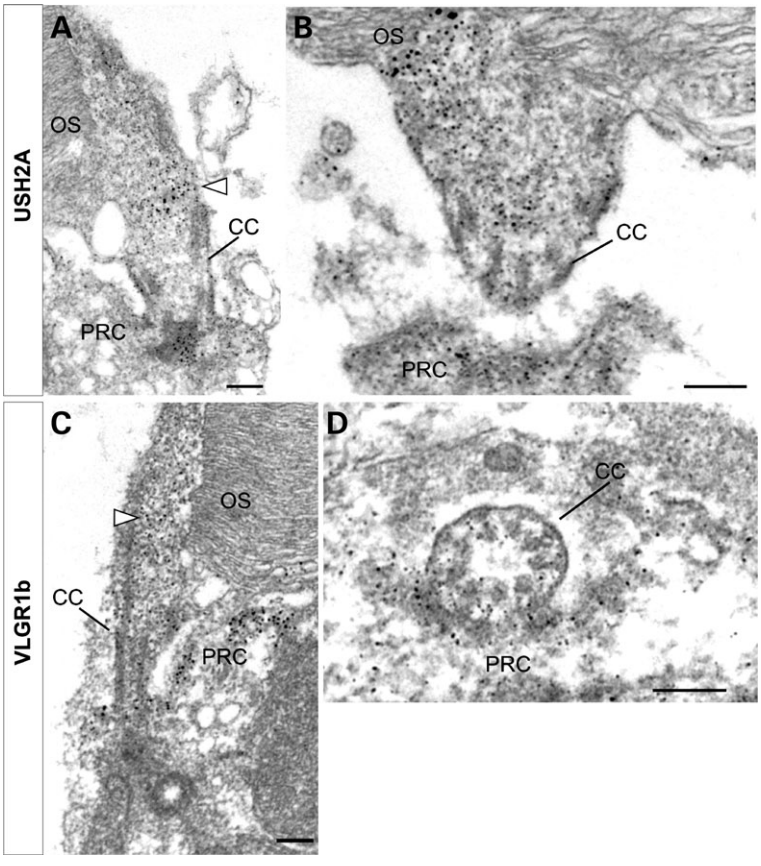

Figure 7. Subcellular localization of USH2A isoform b and VLGR1b in *Xenopus* photoreceptor cells. (**A** and **B**) Electron micrographs of anti-USH2A isoform b labeling in a longitudinal section (A) and an oblique cross-section through the connecting cilium (CC) and the periciliary ridge complex (PRC) (B) of *Xenopus* photoreceptor cells. USH2A isoform b localization is restricted to the apical inner segment in the PRC, at the base of the CC, in the CC, in the basal body complex (BB) and in the axonemal extension of the CC (A) (arrow head). (**C** and **D**) Electron micrographs of anti-VLGR1b-cytoplasmic domain labeling in a longitudinal section (C) and an oblique cross-section through the CC and the PRC (D) of *Xenopus* photoreceptor cells. VLGR1b is detected in the apical inner segment in the PRC at the base of the connecting cilium (CC), in the CC and in the axonemal extension of the CC (arrow head). Scale bars: (A–D) 0.2 μm.

DISCUSSION

USH1 and USH2 proteins are organized in an interactome of multiprotein scaffolds (9,10,16). We and others have identified the USH1C protein harmonin as the major scaffold protein networking USH proteins (9). The localization of all identified components of the USH proteins in the synaptic region of photoreceptor cells indicated the existence of an USH protein network positioned at cone and rod photoreceptor synapses (9). In the present study, we discovered a protein network composed of USH1 and USH2 proteins in the absence of harmonin (Supplementary material Fig. S1) (23) in the periciliary collar of the apical inner segment and the adjacent connecting cilium of mammalian photoreceptor cells. This protein network is organized by two other USH scaffold proteins, namely SANS (USH1G) and whirlin (USH2D) (Fig. 8). In addition, we found an association of SANS with microtubules suggesting an important side branch of USH protein networks to the microtubule cytoskeleton and hence to microtubule-associated intracellular transport processes.

Our yeast two-hybrid screens and subsequent protein–protein interaction assays revealed direct interaction of SANS with whirlin. These findings were confirmed by preliminary data obtained from reciprocal yeast two-hybrid assays using whirlin as bait (14). The validation of this interaction by GST pull-downs demonstrated that SANS binds directly to the PDZ1 and 2, but not to the PDZ3 domain of whirlin. Furthermore, our findings indicate that this interaction is most probably mediated through binding of the C-terminal PBM of SANS. A semi-quantitative analysis of these associations indicates higher affinity of the SANS-C-terminus to PDZ1 than to PDZ2 of whirlin. Nevertheless, the three amino acids of the C-terminal PBM are essential for the interaction of SANS to whirlin's PDZ1 and PDZ2. This is in contrast to the previously identified interaction of SANS with harmonin which is dependent on a larger C-terminal domain of SANS (12).

Several USH1 proteins, namely the cadherins cadherin 23 (USH1D) and protocadherin 15 (USH1F), myosin VIIa (USH1B) and SANS were previously identified as binding partners for whirlin (10,14,16,31). In the latter protein network, whirlin, myosin VIIa and SANS have the potential for homodimerization and interaction with each other (12,31,32). In addition, specific binding of whirlin and myosin VIIa to the large transmembrane proteins USH2A isoform b and VLGR1b was reported (13,14,16). In inner

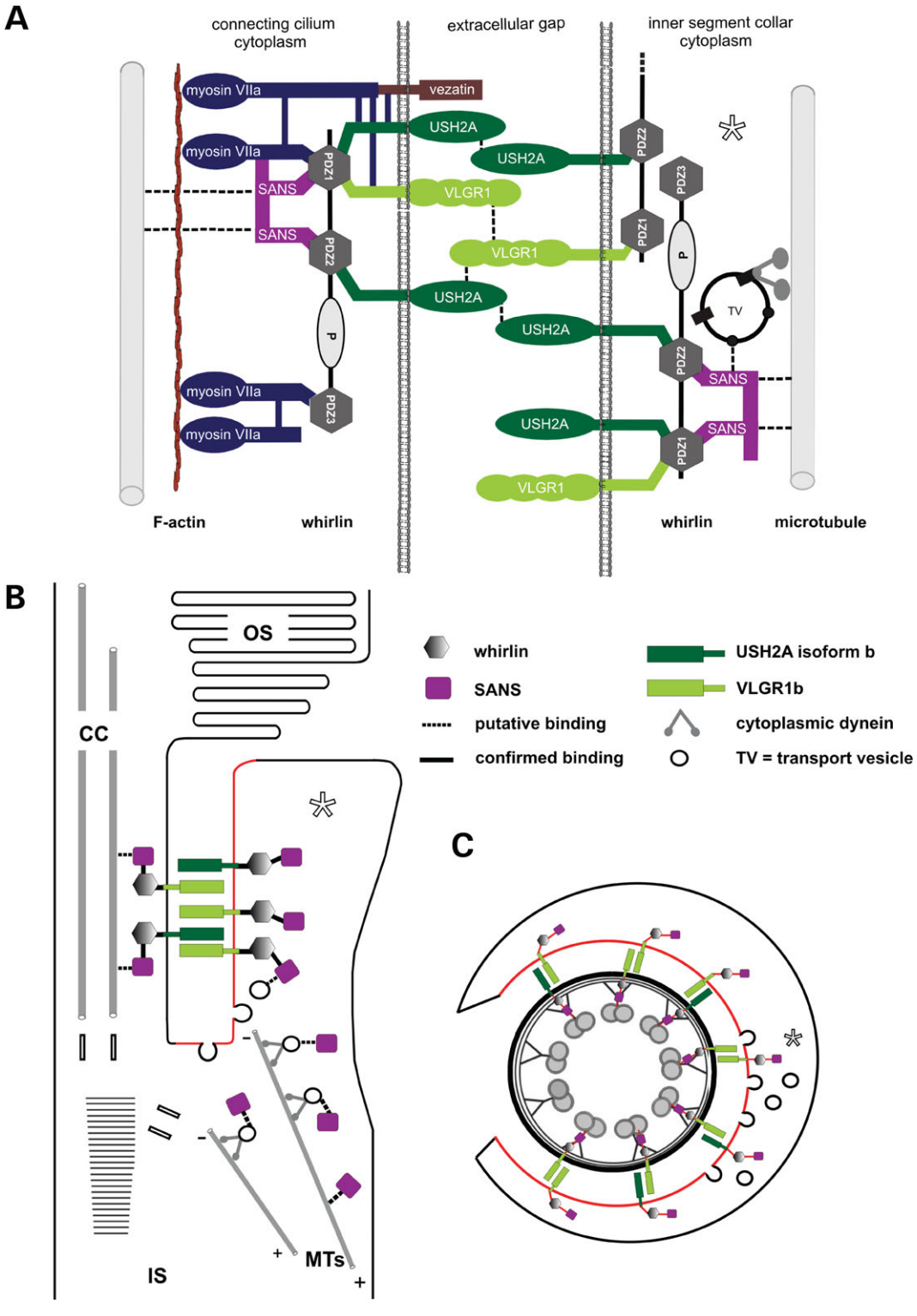

Figure 8. Schematic representation of the protein interactions involved in the ciliary/periciliary protein network of photoreceptor cells. (**A**) Schematic representation of the interactions within ciliary/pericilary protein network. Ectodomains of USH2A isoform b and VLGR1b connect the membranes of the connecting cilium and the inner segment. Both are anchored via whirlin at the USH protein network in the cytoplasm of the adjacent domains. Direct protein–protein interactions are indicated by solid lines. Doted lines indicate putative interaction. Asterisk indicates inner segment collar. (**B** and **C**) Schematic arrangement of the ciliary/periciliary USH protein network and its relation to transport vesicle delivery in a mammalian rod photoreceptor cell. Note: a schematic representation of a *Xenopus* rod cell is presented in the Supplement material Fig. S3. (B) Longitudinal section and (C) Cross-section. Cytoplasmic dynein mediates vesicle transport along microtubules to the apical inner segment collar (asterisk). Docking and fusion membrane sites (indicated in red) are predefined by the USH protein network arrangement.

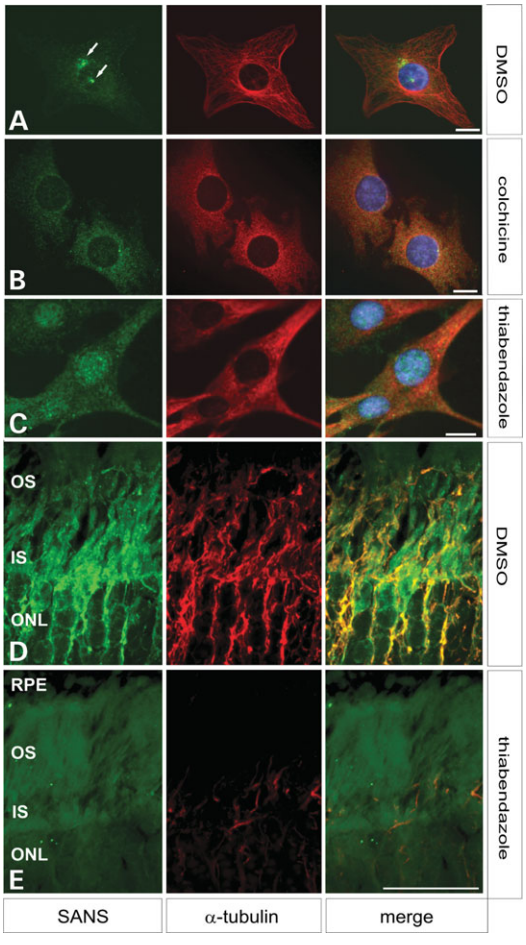

Figure 9. SANS distribution is dependent on microtubules in NIH3T3 cells and organotypic mouse retina culture. (**A**–**C**) SANS distribution after DMSO, colchicine or thiabendazole treatment in NIH3T3 cells. Immunohistochemical localization of SANS (green) and α-tubulin (red) in control cells incubated with DMSO (A) and NIH3T3 cells treated with colchicine (B) or thiabendazole (C). After drug treatment the microtubule network stained by anti-α-tubulin antibodies is destroyed (B and C, middle panels), the anti-SANS punctuated centrosomal labeling (A, left panel, arrows) is abolished and SANS is distributed throughout the cytoplasm (B) or even found in the nucleus (C). (**D** and **E**) SANS distribution in photoreceptor cells after DMSO or thiabendazole treatment of organotypic cultures of mouse retinas. Immunohistochemical localization of SANS (green) and α-tubulin (red) in control retinal cultures incubated with DMSO (D) and after thiabendazole treatment (E). In control retinal cultures, SANS staining overlaps with the microtubule cytoskeleton in photoreceptor cells. After thiabendazole treatment microtubules are depolymerized and SANS distribution is altered and staining intensity is reduced. Scale bars: (A–C) 10 μm and (E) 20 μm.

ear hair cells, several lines of evidence support the hypothesis that a supra-molecular protein complex scaffolded by whirlin plays an important role in the ankle link formation at the base of stereocilia (12–16). These ankle links are extracellular fibrous structures, which connect neighboring stereocilia as well as stereocilia with the adjacent kinocilium, and are essential for correct differentiation and organization of hair cell bundles. Recent data indicated that ankle link fibers are composed of the ectodomains of USH2A isoform b and VLGR1b (13,15,16). It has been suggested that the ankle link complex in hair cells is homologous to the periciliary complex localized to the membranes of the connecting cilium and the collar-like extension of the apical inner segment in photoreceptor cells (15,17,18,33). This is in full agreement with our present data. We show that the molecular composition of the ankle link complex in hair cells and the periciliary complex in photoreceptor cells is conserved. Immunoelectron microscopy demonstrated colocalization of the cytoplasmic domains of the transmembrane proteins USH2A isoform b and VLGR1b with whirlin and SANS in the connecting cilium and in the adjacent apical inner segment collar of mammalian photoreceptor cells. The direct binding to the scaffold protein whirlin most probably anchors both transmembrane proteins within the cytoplasm of these subcellular compartments. The distinct labeling of epitopes by antibodies directed against the ectodomain of VLGR1b in the extracellular gap between the membranes of the cilium and the collar-like extension of the apical inner segment strongly suggests that the extracellular domains of VLGR1b are components of fibrous links, which interconnect adjacent plasma membranes. The absence of these fibers in photoreceptor cells of homozygous Vlgr1/del7TM mice and the BAPTA sensitivity of the ectodomains of VLGR1b further confirmed VLGR1b as an essential component of these fibrous links.

The structures of USH2A isoform b and VLGR1b (see Fig. 1A) are consistent with the hypothesis that both USH2 proteins are substantial components of these fibrous membrane links in vertebrate photoreceptor cells. Estimations of the large ectodomains in both USH2 molecules reveal a length of ~150 nm (13,34) which is in the range of the distance between the ciliary membrane and the adjacent inner segment membrane in photoreceptor cells (>125 nm). There are several possibilities how USH2A isoform b and VLGR1b are arranged within these fibrous links. It is conceivable that USH2A isoform b and VLGR1b form homomers or heteromers mediated by direct interaction of their long ectodomains (13–15). In VLGR1b, CalX-β repeats which are frequently present in the ectodomain were suggested as protein binding domains (15). Such dimerizations may be facilitated through an intracellular tether by parallel binding of their cytoplasmic PBM sites to the PDZ domains 1 and 2 of whirlin. Homo- or heteromers may bridge the extracellular cleft between the adjacent membranes according to mechanisms known from cell–cell adhesion molecules, e.g. conventional cadherins in cell–cell attachments (35). The absence of fibers in homozygous Vlgr1/del7TM mice further indicates that USH2A isoform b homomers are not sufficient for formation and maintenance of these fibers. Nevertheless, recent retinal analyses of USH2A knockout mice demonstrated the essential impact of USH2A isoform b for the maintenance of photoreceptor cell survival (33).

Cell–cell adhesion complexes including membrane-spanning structures supported by cytoplasmic scaffolds often define specialized regions of the plasma membrane. Such organizations are well known from the plasma membrane specializations of the active zone in presynaptic boutons of axons (36) or the division in the apical and baso-lateral membrane of epithelial cells. Present analyses revealed a periciliary USH protein network situated at adjacent membranes of the inner segment collar and the connecting cilium of mouse photoreceptor cells. So far, little was known about

the periciliary structural membrane specialization in the apical inner segment of mammalian photoreceptor cells. In a study, parallel to the present, on USH2A knockout mice (33), it has been suggested that the membrane domain of the apical inner segment collar corresponds to the periciliary ridge complex, previously described by Papermaster and co-workers in amphibian photoreceptor cells (26–28). However, experimental data supporting this hypothesis were non-existent until now. Here, we provide for the first time molecular and ultrastructural evidence indicating the homology between both structures in mammalian and amphibian photoreceptor cells. We demonstrated the localization of the molecular components of the periciliary USH protein network in the connecting cilium and apical inner segment collar in mouse photoreceptor cells and in the periciliary ridge complex of *Xenopus* photoreceptor cells. The USH proteins SANS, whirlin, USH2A isoform b and VLGR1b are localized in the ridges of the periciliary complex and in the connecting cilium of *Xenopus* photoreceptor cells. As in the mouse, extracellular fibrous links project from the tip of each ridge to the membrane of the connecting cilium. These are most probably also composed of the long ectodomains of the transmembrane proteins USH2A isoform b and VLGR1b. As we discussed for mouse photoreceptor cells above, the latter transmembrane proteins may be anchored with their cytodomains via the scaffold proteins whirlin and SANS in the cytoplasm of the two adjacent cellular compartments in *Xenopus* photoreceptor cells. The congruence in the cellular topology and the molecular composition of these membrane-associated periciliary protein complexes strongly supports structural and functional homology in mammalian and *Xenopus* photoreceptor cells.

What is the function of these periciliary complexes in vertebrate photoreceptor cells? In amphibian photoreceptor cells, the membrane subdomains in the grooves of the periciliary ridge complex are thought to constitute docking sites for inner segment transport vesicles, which contain cargo molecules for the outer segment (27,28,37). Independent immunoelectron microscopy analyses revealed association of opsin-laden transport vesicles with the grooves, but not with the ridges (26,27,37–39). These vesicles originate from the *trans*-Golgi network of the cell (4,40). After Golgi budding, cargo vesicles are subsequently transported along microtubules by cytoplasmic dynein to the apical inner segment (2) (Fig. 8B and C). At the apical inner segment membrane, the transport carriers are supposed to dock and fuse with designated plasma membrane domains (4,28,41). In amphibian photoreceptor cells, designated membrane domains are present in the grooves of the periciliary ridge complex (28) (Supplemental material Fig. S3). In mammalian photoreceptors, the membrane domains of the apical inner segment collar localized alongside the connecting cilium correspond to these membrane micro domains (33). In both cases, the USH protein network may structurally support the specialized membrane micro domains by bridging adjacent membranes and anchoring the transmembrane proteins in the cytoplasm of both the inner segment and the connecting cilium.

However, this does not exclude participation of the periciliary protein network in vesicle targeting and guiding as well as in the adjustment of vesicle docking and fusion to designated membrane areas. In particular, the association of SANS with microtubules may affiliate the microtubule routes for the vesicular transport with predefined target membranes in the apical inner segment collar. Indeed previously obtained data indicate that microtubules project into the collar-like extension of the inner segment apex and that cargo vesicles are present at the target membrane (2) (B. Reidel, T. Goldmann, A. Gießl and U. Wolfrum, submitted). Since tethering and fusion of rhodopsin transport carriers is thought to be regulated by phosphatidylinositol-4,5-bisphosphate, moesin, actin and rac1 acting in concert with rab8 (42), future efforts are necessary to provide more insights into molecular links between the structural support function of the USH protein network and transport processes.

In addition, our present data indicate the localization of a USH protein network in the ciliary apparatus of mouse and amphibian photoreceptor cells. In the photoreceptor connecting cilium, SANS may anchor the membrane-associated USH protein network, composed of SANS, whirlin, USH2A isoform b and VLGR1b to the ciliary microtubule doublets. A solid SANS association with the ciliary cytoskeleton of photoreceptor cells was recently confirmed by the recovery of SANS in the detergent insoluble cytoskeleton fraction of enriched photoreceptor cilia (29). Furthermore, the USH1B protein myosin VIIa is capable of direct binding to all proteins of the present network (12,16).

The molecular motor myosin VIIa can have a dual function in the connecting cilium: after the fusion of membranous vesicles with the apical surface of the inner segment discussed above, the membrane incorporated cargo translocates in the ciliary membrane to the outer segment. We previously indicated that myosin VIIa mediates the transport of membrane cargo along actin filaments in the membrane of photoreceptor cilia (3). The direct binding of myosin VIIa to the proteins of the ciliary USH protein network may connect this transport system through SANS to the prominent microtubule cytoskeleton of the cilium (29). Furthermore, the regulation of myosin VIIa mediated molecular trafficking by the interaction with SANS was previously suggested for the delivery of proteins to stereovilli in inner ear hair cells (12).

However, myosin VIIa and the transmembrane protein vezatin, identified as one of the first interaction partners of myosin VIIa, are present in the connecting cilium (43) (u. Wolfrum unpublished data) and directly interact with the cytoplasmic domains of transmembrane proteins USH2A isoform b and VLGR1b (16). Thus, it has to be considered that the motor protein myosin VIIa could actively support the protein network at the ciliary membrane by force generation at the cytoplasmic domains of the transmembrane proteins (43).

In conclusion, our data show that an USH protein network is localized at the interface of the inner segment and the light sensitive outer segment of rod and cone vertebrate photoreceptor cells. The cooperation of the network members may contribute to the regulation of cargo transfer from inner segment transport carriers to the ciliary transport system. Dysfunction or absence of any of the proteins in the ciliary–periciliary USH protein network may lead to the disruption of the entire network function and may cause degeneration of the neuronal retina, the clinical retinal symptom characteristic for USH patients.

MATERIALS AND METHODS

Yeast two-hybrid assays

The GAL4-based yeast two-hybrid system (HybriZAP, Stratagene, La Jolla, USA) was used to identify the interactions between SANS, whirlin and putative interactors as previously described (44). The DNA-binding domain (pBD) fused to either the SAMPBM domain of SANS, or PDZ1 and 2 or PDZ3 of whirlin respectively, was used as a bait on a bovine oligo-dT primed retinal cDNA library. The yeast strain *PJ69-4A* was used as a host, which carried the *HIS3* (histidine), *ADE2* (adenine), *MEL1* (α-galactosidase) and *LacZ* (β-galactosidase) reporter genes. Interactions were analyzed by assessment of reporter gene activation, using growth on selective media (*HIS3* and *ADE2* reporter genes), X-α-gal colorimetric plate assays (*MEL1* reporter gene) and X-β-gal colorimetric filter lift assays (*LacZ* reporter gene). To map the interacting domains of SANS and whirlin, constructs fused to the DNA-activation domain and pBD were cotransformed in *PJ694α*. If yeast clones grew on selection plates and were stained in the α- and β-galactosidase activity assays, an interaction between a protein pair was indicated.

GST pull-down assays

Constructs encoding human whirlin domains were cloned in the pDEST15 vector (Gateway cloning system, Invitrogen, Karlsruhe, Germany). GST-fusion proteins were produced by transforming BL21-DE3 cells with pDEST15-whirlin PDZ1 (amino acids 45–141), PDZ2 (187–268), PDZ 1+2 (45–268) and PDZ3 (469–814). Cells were induced at 30°C with 0.5 mM IPTG overnight and subsequently lysed with STE buffer [1% Sarkosyl, 1% Triton-X-100, 5 mM 1,4-dithiothreitol (DTT)] supplemented with complete protease inhibitor cocktail (Roche Diagnostics, Mannheim, Germany). Lysates were incubated with glutathione–sepharose 4B beads (Amersham Biosciences, Freiburg, Germany). The GST-fusion proteins bound to the beads were washed with lysis buffer and TBSTD (TBS with 1% Triton-X-100 and 2 mM DTT). The amount of bound GST-fusion protein was verified on a NUPAGE Novex 4–12% Bis-Tris SDS–PAGE gel and stained with SimplyBlue SafeStain (Invitrogen). FLAG-tagged human SANS full length (amino acids 1–461) and FLAG-tagged SANS SAMΔPBM (amino acids 385–455) were produced by transfection of COS-1 cells with the appropriate vectors, using Effectene as a transfection reagent (QIAGEN, Hilden, Germany) according to the manufacturer's instruction. Twenty-four hours after transfection cells were washed with PBS and subsequently lysed on ice in lysis buffer (50 mM Tris–HCL pH 7.5, 150 mM NaCl, 0.5% Triton-X-100). The cell supernatant was incubated overnight at 4°C with equal amounts of beads pre-incubated either with GST or with GST-fusion proteins. Beads were washed and precipitated protein complexes were eluted with SDS sample buffer and subjected to SDS–PAGE and western blot analysis.

Animals and tissue preparation

All experiments conformed to the statement by the Association for Research in Vision and Ophthalmology (ARVO) regarding the care and use of animals in research. Mature C57BL/6J and Vlgr1/del7TM mice, previously described by McMillan and White (24), and adult *X. laevis* were maintained on a 12-h light–dark cycle, with food and water *ad libitum*. After sacrifice of the animals by sodium pentobarbital overdoses (mice) or chloroform (*Xenopus*) and decapitation, subsequently entire eyeballs were dissected or retinas were removed through a slit in the cornea prior to further analyses.

Fluorescence microscopical analysis of cotransfected COS-1 cells

Full-length whirlin was cloned in pDEST 733 resulting in an N-terminal-fused mRFP and full-length SANS was cloned in pDEST 501 resulting in an N-terminal-fused eCFP-protein. Both constructs were transfected individually or in combination by using Effectene transfection reagent (QIAGEN) according to the manufacturer's instructions. After 24 h cells were washed in PBS and fixed with 3.7% paraformaldehyde (PFA), mounted with vectashield containing DAPI (4',6-Diamidin-2'-phenylindoldihydrochlorid) (Vector Laboratories Inc., Peterborough, UK) and analyzed by epifluorescence microscopy.

Coimmunoprecipitation

Retina lysate was prepared in HNTG buffer (20 mM Hepes, 150 mM NaCl, 0.1% Triton-X-100, 6 mM EDTA, 10% glycerol, pH 7.4). 35 μl AG-Beads (PIERCE, Rockford, USA) were washed with HNTG buffer and displaced with 5 μl anti-whirlin antibodies per reaction. As a negative control beads were incubated without antibodies. All mixtures were incubated at 4°C for 4–5 h. To remove unbound antibodies beads were washed several times with HNTG buffer. Afterwards retina extracts were applied to the beads in equal amounts and incubated at 4°C overnight. Beads were washed and precipitated protein complexes were eluted with SDS sample buffer and subjected to SDS–PAGE and western blot analysis.

Western blot analyses

For western blot analyses, the appropriate tissues were homogenized in buffer containing a protease inhibitor cocktail (Roche Diagnostics). Samples were prepared in either RIPA buffer (50 mM Tris–HCl, 150 mM NaCl, 0.1% SDS, 2 mM EDTA, 1% NP-40, 0.5% sodium-deoxycholate, 1 mM sodium-vanadate, 30 mM sodium-pyrophosphate, pH 7.4) or HNTG buffer (20 mM Hepes, 150 mM NaCl, 0.1% Triton-X-100, 6 mM EDTA, 10% glycerol, pH 7.4). For denaturing gel electrophoresis, samples were mixed with SDS–PAGE sample buffer (62.5 mM Tris–HCl, 10% glycerol, 2% SDS, 5% mercaptoethanol, 1 mM EDTA and 0.025 mM bromphenol blue, pH 6.8). 25 μg protein extract per lane was separated on a 12% polyacrylamide gel and transferred onto polyvinylidene difluoride membranes (Millipore, Schwalbach, Germany). After blocking the membrane with Applichem blocking reagent (Applichem, Darmstadt, Germany) for 2 h at room temperature, immunoreactivities were detected by applying primary and appropriate secondary antibodies (IRDye 680 or

800, Rockland, Gilbertsville, USA) employing the Odyssey infrared imaging system (LI-COR Biosciences, Lincoln, USA). As a molecular marker a prestained ladder (Sigma-Aldrich, Deisenhofen, Germany) was used, ranging from 11–170 kDa.

Constructs for expression of cDNA

cDNAs for expression of proteins were obtained by RT–PCR or from EST-clones and subcloned into the appropriate expression vectors as previously described (14,23). The numbers of the given amino acids are according to the following Genbank entries. SANS (murine) AF_176847, SANS (human) AF_775748, USH2A isoform b (human), NP_99681, VLGR1b (human) and NP_115495.

Antibodies and fluorescent dyes

Polyclonal antibodies against SANS generated against a murine fragment (amino acids 1–46) and raised in rabbit were previously characterized (29). The anti-whirlin antibodies were raised in guinea pig against a GST-fusion protein encoding the human amino acid region 701–765 of the long isoform of whirlin (14). The antibodies against VLGR1b were either generated against the cytoplasmic tail (amino acids 6198–6307) (24) or against a GST-fusion protein of the extracellular region (amino acids 3249–3425) (kindly provided by Dr Dominic Cosgrove, Omaha, USA) both of murine origin and raised in rabbit. Anti-USH2A antibodies were generated against fibronectin (FN) type III domains of mouse USH2A (amino acids 1359–1443) raised in guinea pig and against a 139 amino acids fragment encoding the cytoplasmic tail of human USH2A, raised in rabbit (24). Monoclonal antibodies against centrins (clone 20H5, detecting all four centrin isoforms) have previously been characterized (45). Specific antibodies against harmonin (amino acids 1–89) raised in rabbit were characterized before (23). Expression of the fusion proteins and purification of the antibodies were performed as previously described (23). The anti-α-tubulin and anti-FLAG-tag antibodies were acquired from Sigma-Aldrich. The secondary antibodies were purchased from Invitrogen or Rockland.

Immunofluorescence microscopy

Eyes of adult wild-type mice were cryofixed in melting isopentane and cryosectioned as described elsewhere (46). Cryosections were placed on poly-*L*-lysine-precoated coverslips and incubated subsequently with 0.01% Tween 20 in PBS for 20 min. After several PBS washing steps sections were covered with blocking solution (0.5% cold-water fish gelatin plus 0.1% ovalbumin in PBS) and incubated for a minimum of 30 min followed by an overnight incubation with primary antibodies, diluted in blocking solution at 4°C. Washed cryosections were incubated with secondary antibodies conjugated to Alexa 488 or Alexa 568 (Invitrogen) in PBS with DAPI (Sigma-Aldrich) to stain the DNA of the cell nuclei, for a minimum of 1.5 h at room temperature in the dark. After repeated washing with PBS sections were mounted in Mowiol 4.88 (Hoechst, Frankfurt, Germany). Mounted retina cryosections were analyzed by microscopy (DMRB; Leica microsystems, Bensheim, Germany). Images were obtained with a charge-coupled device camera (ORCA ER; Hamamatsu, Herrsching, Germany) and processed with Adobe Photoshop CS (Adobe Systems, San Jose, USA).

Immunoelectron microscopy

Isolated mouse and *Xenopus* eye balls were placed in 4% PFA in Soerensen buffer (0.1 M disodiumhydrogenphophate, 0.1 M potassiumdihydrogenphosphate, pH 7.3), perforated with an injection needle and the lens was removed. Then the eyecups were prefixed in 4% in 0.1 M Soerensen buffer (pH 7.3) for 50 min. After washing in Soerensen buffer retinas were dissected from the eyecups in 10% sucrose in Soerensen buffer from the eyecups and incubated in 10 and 20% sucrose in Soerensen buffer for 2 h in each case and in 30% sucrose in Soerensen buffer overnight. In one experiment, we dissected the retina in PBS and treated it with 0.5% Triton in PBS for 3 min. After that the retina was fixed for 50 min in 4% PFA and further treated as above. After four cycles of freezing (−196°C) and thawing (37°C) the retinas were washed in PBS and embedded in buffered 2% Agar (Sigma-Aldrich). Agar blocks were sectioned by a vibratome (Leica, Wetzlar, Germany) in 50 μm slices. Vibratome sections were blocked for 2 h in 10% normal goat serum (NGS), 1% bovine serum albumin (BSA) in PBS and subsequently incubated with primary antibodies against SANS, whirlin, USH2A isoform b, VLGR1b or harmonin in 3% NGS, 1% BSA in PBS for 4 days at 4°C. After washing with PBS the appropriate biotinylated secondary antibodies (Vector Laboratories) were applied to the sections for 2 h at room temperature. Following several washing steps with PBS, a complex consisting of avidin and biotinylated horseradish peroxidase (Vectastain ABC-Kit, Vector Laboratories) was added to the sections and incubated for 1.5 h in the dark. After incubation with diaminobenzidine the precipitate was fixed in 2.5% glutaraldehyde in 0.1 M Cacodylate buffer (pH 7.3) for 1 h. After silver enhancement sections were fixed in 0.5% OsO_4 in 0.1 M Cacodylate buffer (pH 7.3) on ice, dehydrated and embedded in araldite. Ultrathin sections were cut and microscopical analysis was performed using a Tecnai 12 BioTwin transmission electron microscope (FEI, Eindhoven, NL).

BAPTA treatment

To examine the effects of the calcium chelator BAPTA (1,2-bis(o-aminophenoxy)ethane-N,N,N',N'-tetraacetic acid) (Sigma-Aldrich) mouse retina cryosections were incubated with Ca^{2+}-free PBS containing 5 mM BAPTA for 30 min at room temperature. After BAPTA incubation of cryosections were washed several times with PBS and processed for immunofluorescence microscopy as described above.

Organotypic retina culture

The elaboration of the retina culture system was previously described (30). Intact eyes removed from sacrificed C57BL/6J mice on post-natal day 16–19 were incubated in

1.2 mg/ml proteinase K (Sigma-Aldrich) for 15 min at 37°C. Proteinase K activity was stopped by application of Dulbecco's Modified Eagle's Medium with F12 supplement (DMEM–F12) with 10% fetal calf serum for 5 min. After rinsing the eyes in serum-free medium retinas were dissected following removal of the sclera, the ocular tissue and the hyaloid vessel. Specimens were cultured with the retinal pigmented epithelial cells facing down on ME 25/31 culture membranes (Whatman, Dassel, Germany) in DMEM–F12 and 10% fetal calf serum, L-glutamine, penicillin and streptomycin (Sigma-Aldrich) at 37°C in a 5% CO_2 atmosphere. Retinas were mounted and frozen as previously described (30) and processed for immunofluorescence microscopy as described above.

Application of cytoskeletal drugs

Thiabendazole (Fluka, Seelze, Germany) and colchicine (Sigma-Aldrich) were diluted in 1% DMSO. The applied end concentration of thiabendazole was 1.5 mM to organotypic retina culture medium and 0.5 mM to NIH3T3 cell culture medium; colchicine was applied in an end concentration of 125 nM to NIH3T3 cell culture medium for 2 h at 37°C and 5% CO_2. Controls were incubated with 1% DMSO under the same conditions and processed as described for organotypic retina culture.

SUPPLEMENTARY MATERIAL

Supplementary Material is available at HMG Online.

ACKNOWLEDGEMENTS

Authors thank Gabi Stern-Schneider and Ulrike Maas for technical assistance, Dr Dominic Cosgrove (Boys Town National Research Hospital, Omaha, NE) for providing us with anti-VLGR1b antibodies and Drs Kerstin Nagel-Wolfrum and Martin Latz for critical reading of the manuscript.

Conflict of Interest statement. None declared.

FUNDING

This work was supported by the DFG (to U.W.), Forschung contra Blindheit—Initative Usher Syndrom (to H.K., T.M. and U.W.), ProRetina Deutschland (to U.W.), the FAUN-Stiftung, Nürnberg (U.W.), the Nijmegen ORL Research Fund (to H.K.), the Heinsius Houbolt Foundation (to H.K.) the BRPS (to H.K. and R.R) and the NIH EY016247 (to Perrin White, E.J.W. and J.M.).

REFERENCES

1. Young, R.W. (1976) Visual cells and the concept of renewal. *Invest. Ophthalmol. Vis. Sci.*, **15**, 700–725.
2. Tai, A.W., Chuang, J.Z., Bode, C., Wolfrum, U. and Sung, C.H. (1999) Rhodopsiń s carboxy-terminal cytoplasmic tail acts as a membrane receptor for cytoplasmic dynein by binding to the dynein light chain Tctex-1. *Cell*, **97**, 877–887.
3. Wolfrum, U. and Schmitt, A. (2000) Rhodopsin transport in the membrane of the connecting cilium of mammalian photoreceptor cells. *Cell Motil. Cytoskeleton*, **46**, 95–107.
4. Deretic, D. (2006) A role for rhodopsin in a signal transduction cascade that regulates membrane trafficking and photoreceptor polarity. *Vision Res.*, **46**, 4427–4433.
5. Roepman, R. and Wolfrum, U. (2007) Protein networks and complexes in photoreceptor cilia. Faupel, M. and Bertrand, E. (eds), *Subcellular Fractionation and Proteomics*, Springer, NY.
6. Petit, C. (2001) Usher syndrome: from genetics to pathogenesis. *Annu. Rev. Genomics Hum. Genet.*, **2**, 271–297.
7. Ahmed, Z.M., Riazuddin, S., Riazuddin, S. and Wilcox, E.R. (2003) The molecular genetics of Usher syndrome. *Clin. Genet.*, **63**, 431–444.
8. Davenport, S.L.H. and Omenn, G.S. (1977) The heterogeneity of Usher syndrome. Vth Int. Conf. Birth Defects, Montreal.
9. Reiners, J., Nagel-Wolfrum, K., Jurgens, K., Märker, T. and Wolfrum, U. (2006) Molecular basis of human Usher syndrome: deciphering the meshes of the Usher protein network provides insights into the pathomechanisms of the Usher disease. *Exp. Eye Res.*, **83**, 97–119.
10. Kremer, H., van Wijk, E., Märker, T., Wolfrum, U. and Roepman, R. (2006) Usher syndrome: molecular links of pathogenesis, proteins and pathways. *Hum. Mol. Genet.*, **15**, 262–270.
11. Ebermann, I., Scholl, H.P., Charbel, I.P., Becirovic, E., Lamprecht, J., Jurklies, B., Millan, J.M., Aller, E., Mitter, D. and Bolz, H. (2007) A novel gene for Usher syndrome type 2: mutations in the long isoform of whirlin are associated with retinitis pigmentosa and sensorineural hearing loss. *Hum. Genet.*, **121**, 203–211.
12. Adato, A., Michel, V., Kikkawa, Y., Reiners, J., Alagramam, K.N., Weil, D., Yonekawa, H., Wolfrum, U., El Amraoui, A. and Petit, C. (2005) Interactions in the network of Usher syndrome type 1 proteins. *Hum. Mol. Genet.*, **14**, 347–356.
13. Adato, A., Lefevre, G., Delprat, B., Michel, V., Michalski, N., Chardenoux, S., Weil, D., El Amraoui, A. and Petit, C. (2005) Usherin, the defective protein in Usher syndrome type IIA, is likely to be a component of interstereocilia ankle links in the inner ear sensory cells. *Hum. Mol. Genet.*, **14**, 3921–3932.
14. van Wijk, E., van der Zwaag, B., Peters, T., Zimmermann, U., te Brinke, H., Kersten, F.F., Märker, T., Aller, E., Hoefsloot, L.H., Cremers, C.W. *et al.* (2006) The DFNB31 gene product whirlin connects to the Usher protein network in the cochlea and retina by direct association with USH2A and VLGR1. *Hum. Mol. Genet.*, **15**, 751–765.
15. McGee, J., Goodyear, R.J., McMillan, D.R., Stauffer, E.A., Holt, J.R., Locke, K.G., Birch, D.G., Legan, P.K., White, P.C., Walsh, E.J. *et al.* (2006) The very large G-protein-coupled receptor VLGR1: a component of the ankle link complex required for the normal development of auditory hair bundles. *J. Neurosci.*, **26**, 6543–6553.
16. Michalski, N., Michel, V., Bahloul, A., Lefevre, G., Barral, J., Yagi, H., Chardenoux, S., Weil, D., Martin, P., Hardelin, J.P. *et al.* (2007) Molecular characterization of the ankle-link complex in cochlear hair cells and its role in the hair bundle functioning. *J. Neurosci.*, **27**, 6478–6488.
17. Goodyear, R. and Richardson, G. (1999) The ankle-link antigen: an epitope sensitive to calcium chelation associated with the hair-cell surface and the calycal processes of photoreceptors. *J. Neurosci.*, **19**, 3761–3772.
18. Goodyear, R.J. and Richardson, G.P. (2003) A novel antigen sensitive to calcium chelation that is associated with the tip links and kinocilial links of sensory hair bundles. *J. Neurosci.*, **23**, 4878–4887.
19. Wolfrum, U. (1995) Centrin in the photoreceptor cells of mammalian retinae. *Cell Motil. Cytoskeleton*, **32**, 55–64.
20. Gießl, A., Pulvermüller, A., Trojan, P., Park, J.H., Choe, H.W., Ernst, O.P., Hofmann, K.P. and Wolfrum, U. (2004) Differential expression and interaction with the visual G-protein transducin of centrin isoforms in mammalian photoreceptor cells. *J. Biol. Chem.*, **279**, 51472–51481.
21. Besharse, J.C. and Horst, C.J. (1990) The photoreceptor connecting cilium—a model for the transition zone. Bloodgood, R.A. (Ed.), *Ciliary and Flagellar Membranes*. Plenum, New York, pp. 389–417. pp.
22. Pagh-Roehl, K., Wang, E. and Burnside, B. (1992) Shortening of the calycal process actin cytoskeleton is correlated with myoid elongation in teleost rods. *Exp. Eye Res.*, **55**, 735–746.
23. Reiners, J., Reidel, B., El Amraoui, A., Boeda, B., Huber, I., Petit, C. and Wolfrum, U. (2003) Differential distribution of harmonin isoforms and their possible role in Usher-1 protein complexes in mammalian photoreceptor cells. *Invest. Ophthalmol. Vis. Sci.*, **44**, 5006–5015.

24. Reiners, J., van Wijk, E., Märker, T., Zimmermann, U., Jurgens, K., te Brinke, H., Overlack, N., Roepman, R., Knipper, M., Kremer, H. *et al.* (2005) Scaffold protein harmonin (USH1C) provides molecular links between Usher syndrome type 1 and type 2. *Hum. Mol. Genet.*, **14**, 3933–3943.
25. McMillan, D.R. and White, P.C. (2004) Loss of the transmembrane and cytoplasmic domains of the very large G-protein-coupled receptor-1 (VLGR1 or Mass1) causes audiogenic seizures in mice. *Mol. Cell Neurosci.*, **26**, 322–329.
26. Peters, K.R., Palade, G.E., Schneider, B.G. and Papermaster, D.S. (1983) Fine structure of a periciliary ridge complex of frog retinal rod cells revealed by ultrahigh resolution scanning electron microscopy. *J. Cell Biol.*, **96**, 265–276.
27. Papermaster, D.S., Schneider, B.G., DeFoe, D. and Besharse, J.C. (1986) Biosynthesis and vectorial transport of opsin on vesicles in retinal rod photorecptors. *J. Histochem. Cytochem.*, **34**, 5–16.
28. Papermaster, D.S. (2002) The birth and death of photoreceptors: the Friedenwald Lecture. *Invest. Ophthalmol. Vis. Sci.*, **43**, 1300–1309.
29. Overlack, N., Märker, T., Latz, M., Nagel-Wolfrum, K. and Wolfrum, U. (2007) SANS (USH1G) expression in developing and mature mammalian retina. *Vision Res.*, 2007 Oct 6; (Epub ahead of print).
30. Reidel, B., Orisme, W., Goldmann, T., Smith, C.W. and Wolfrum, U. (2006) Photoreceptor vitality in organotypic cultures of mature vertebrate retinas validated by light-dependent molecular movements. *Vision Res.*, **46**, 4464–4471.
31. Delprat, B., Michel, V., Goodyear, R., Yamasaki, Y., Michalski, N., El Amraoui, A., Perfettini, I., Legrain, P., Richardson, G., Hardelin, J.P. *et al.* (2005) Myosin XVa and whirlin, two deafness gene products required for hair bundle growth, are located at the stereocilia tips and interact directly. *Hum. Mol. Genet.*, **14**, 401–410.
32. Udovichenko, I.P., Gibbs, D. and Williams, D.S. (2002) Actin-based motor properties of native myosin VIIa. *J. Cell Sci.*, **115**, 445–450.
33. Liu, X., Bulgakov, O.V., Darrow, K.N., Pawlyk, B., Adamian, M., Liberman, M.C. and Li, T. (2007) Usherin is required for maintenance of retinal photoreceptors and normal development of cochlear hair cells. *Proc. Natl. Acad. Sci. USA*, **104**, 4413–4418.
34. McMillan, D.R., Kayes-Wandover, K.M., Richardson, J.A. and White, P.C. (2002) Very large G protein-coupled receptor-1, the largest known cell surface protein, is highly expressed in the developing central nervous system. *J. Biol. Chem.*, **277**, 785–792.
35. Bolz, H., Reiners, J., Wolfrum, U. and Gal, A. (2002) The role of cadherins in Ca^{2+}-mediated cell adhesion and inherited photoreceptor degeneration. *Adv. Exp. Med. Biol.*, **514**, 399–410.
36. Zhen, M. and Jin, Y. (2004) Presynaptic terminal differentiation: transport and assembly. *Curr. Opin. Neurobiol.*, **14**, 280–287.
37. Papermaster, D.S., Schneider, B.G. and Besharse, J.C. (1985) Vesicular transport of newly synthesized opsin from the Golgi apparatus toward the rod outer segment. *Invest. Ophthalmol. Visual Sci.*, **26**, 1386–1404.
38. Besharse, J.C. and Pfenninger, K.H. (1980) Membrane assembly in retinal photoreceptors. I. Freeze-fracture analysis of cytoplasmic vesicles in relationship to disc assembly. *Cell Biol.*, **87**, 451–463.
39. Schneider, B.G. and Papermaster, D.S. (1983) Immunocytochemistry of retinal membrane protein biosynthesis at the electron microscopic level by the albumin embedding technique. *Methods Enzymol.*, **96**, 485–495.
40. Deretic, D., Williams, A.H., Ransom, N., Morel, V., Hargrave, P.A. and Arendt, A. (2005) Rhodopsin C terminus, the site of mutations causing retinal disease, regulates trafficking by binding to ADP-ribosylation factor 4 (ARF4). *Proc. Natl. Acad. Sci. USA*, **102**, 3301–3306.
41. Sung, C.H. and Tai, A.W. (2000) Rhodopsin trafficking and its role in retinal dystrophies. *Int. Rev. Cytol.*, **195**, 215–267.
42. Deretic, D., Traverso, V., Parkins, N., Jackson, F., Rodriguez de Turco, E.B. and Ransom, N. (2004) Phosphoinositides, ezrin/moesin, and rac1 regulate fusion of rhodopsin transport carriers in retinal photoreceptors. *Mol. Biol. Cell*, **15**, 359–370.
43. Küssel-Andermann, P., El-Amraoui, A., Safieddine, S., Nouaille, S., Perfettini, I., Lecuit, M., Cossart, P., Wolfrum, U. and Petit, C. (2000) Vezatin, a novel transmembrane protein, bridges myosin VIIA to the cadherin-catenins complex. *EMBO J.*, **19**, 6020–6029.
44. Roepman, R., Schick, D. and Ferreira, P.A. (2000) Isolation of retinal proteins that interact with retinitis pigmentosa GTPase regulator by interaction trap screen in yeast. *Methods Enzymol.*, **316**, 688–704.
45. Wolfrum, U. and Salisbury, J.L. (1998) Expression of centrin isoforms in the mammalian retina. *Exp. Cell Res.*, **242**, 10–17.
46. Wolfrum, U. (1991) Tropomyosin is co-localized with the actin filaments of the scolopale in insect sensilla. *Cell Tissue Res.*, **265**, 11–17.